RSC Advances

ROYAL SOCIETY OF CHEMISTRY

www.rsc.org/advances

Effect of Li^+ ion on multimodal emission of lanthanide doped phosphor

R. V. Yadav[1], S. K. Singh[2,*] S. B. Rai[1]

[1]*Department of Physics, Banaras Hindu University, Varanasi-221005, India*

[2]*Department of Physics, Indian Institute of Technology (Banaras Hindu University), Varanasi-221005, India*

Abstract

Present study probes the multimodal emission: upconversion (UC), photoluminescence (PL) and quantum cutting (QC) processes in Ho^{3+}/Yb^{3+} co-doped Y_2O_3 phosphor and further examines the impact of Li^+ ion on the multi-modal emission, for the first time. Materials give efficient emission in green region both through UC and PL, while efficient NIR emission is observed through QC process. Co-operative energy transfer (CET) have been ascribed as the possible mechanism for QC; as result of which a UV/blue photon absorbed by Ho^{3+} ion splits into two near infrared photons (wavelength range 950-1000 nm) emitted by Yb^{3+} ion pair. The Yb^{3+} concentration dependent ET efficiency and QC efficiency has also been evaluated. The energy transfer from Ho^{3+} to Yb^{3+} has been calculated whose efficiency is around 82%, and so, the corresponding QC efficiency is 182%. Co-doping of Li^+ ion has been found capable to enhance the efficiency of QC emission for about 8%, similar to that of UC and PL emission, and hence the multimodal emission is enhanced. Such NIR QC phosphors have great promises in energy conversion for c-Si solar cell applications.

Keywords: Lanthanide, lithium ion, phosphor, quantum-cutting

---

[*]**Corresponding author: Tel.:** *+91 8574027822;* ***E-mail address:*** sunilcfsl@gmail.com, sunilks.app@itbhu.ac.in (S. K. Singh)

1.0 Introduction

Lanthanide doped phosphors have been of great interest owing to their captivating applications in numerous fields including lighting, opto-electronic gadgets, security and flagging, medicinal diagnostics, etc.[1-6] Recent research on these phosphors is broadly covering two principle areas, namely bio-imaging and energy harvesting. In the bio-imaging research, upconversion (UC) property of lanthanide nano-particle is used as it is expected to enhance the bio-imaging from various perspectives including penetration depth, lower scattering, negligible auto-fluorescence, high signal-to-noise ratio, etc.[7-13] On the other hand, the second appealing application, i.e. energy harvesting, fully utilizes the unique multi-modal (fluorescence (PL), UC and downconversion/quantum-cutting (QC)) emission characteristics of lanthanide ions.[14-17] The conversion efficiency of silicon solar cells for UV (250-400 nm) and IR sub-band gap i.e. beyond 1100 nm) radiation is extremely poor. Lanthanides by their property of UV to visible and/or NIR QC, and through the process of infrared to visible UC can make use of the complete solar spectrum in better ways.[18-20] Thus, lanthanide doped phosphor capable of multi-modal emission is new trust for solar cell research and are being actively explored.

In a broad sense, practically all the lanthanide ions with the exception of La, which don't have 4f electron, and Lu, which has 14 electrons, all the orbital are completely filled and so it is not useful as an activator ion, are well known for their conceivable PL in UV-Vis-NIR region. However, when it comes to UC, particularly by infrared excitation, the number of lanthanide ions is considerably reduced. Further, for realization of all the three optical processes, i.e. for multi-mode emission, just a couple of lanthanides (Tb, Tm, Ho and Eu), either separately or co-doped with Yb, stay in picture. However, it doesn't imply that, selecting these lanthanides in any host matrix ensures an effective multimodal emission. Herein, it is worthwhile to mention that, QC is not as basic as PL and UC and needs certain

prerequisite amid the choice of host (e.g. low phonon recurrence) and activator ion. As of late, few articles have been published on multimodal emission behaviour of lanthanide doped phosphors including our own particular work, but the area is very less explored and needs further extensive research.[21-23]

Herein, in this study, we have observed multimodal emission in Ho^{3+}/Yb^{3+} co-doped Y_2O_3 phosphor and further examined the impact of Li^+ ion on the multi-modal emission, for the first time. Doping of cations (such as Li^+, Na^+, K^+, etc.) into phosphor framework has been considered truly successful. The Li^+ ion has the smallest cationic radius in the periodical table of elements, which is quite favourable for their movement and site occupation in the host lattice and thereby changes the crystal field appreciably. These preferences make them appealing for their use in tailoring of the host lattice local crystal field, particularly the host lattices doped with lanthanide ions.[24,25] Electronic-dipole transitions due to 4f levels in lanthanide ions are forbidden by Laporte selection rules. These transitions become partially allowed by the involvement of local crystal field around the lanthanide ions, due to the capability of lanthanide ions to intermix with their states of odd parity.[24] As a result of this intermixing, the local crystal field of the lanthanide ions is tailored and consequently radiative parameters are changed obviously, which turn out to be an extra methodology to change the luminescence. Therefore, effect of Li^+ ions has been explored broadly on PL and UC properties, but there is no report on its effect on QC property of lanthanides.

2. Experimental

2.1 Material and Synthesis

Yttrium oxide (Y_2O_3, 99.99%, Himedia), holmium oxide (Ho_2O_3, 99.9%, Moly Chem), ytterbium oxide (Yb_2O_3, 99.99%, Alfa Aesar), nitric acid (Merck) and urea (Fisher Scientific) were used as starting material for synthesis. The phosphor (with compositional formula $Y_{2-x-y}Ho_xYb_yO_3$) was prepared by using solution combustion technique.[26] In the first step, material

was optimized for 1 mol% Ho^{3+} (x=0.01) and then different concentration of Yb^{3+} (y = 0.00, 0.05, 0.10, 0.15) was tried. Further, $Y_{1.94}Ho_{0.01}Yb_{0.05}O_3$ phosphor was then doped with varying concentration of Li^+ (z = 0.00, 0.03, 0.05, 0.10) in addition. Initially, metal nitrates were prepared by dissolving the oxides in nitric acid and then urea is added as fuel, and mixture is stirred in a beaker to get a homogeneous transparent solution. The solution is then heated at 60 ^oC to get a transparent gel, which is allowed for auto ignition inside a close furnace maintained at 600 ^oC. The obtained foam like product was then grinded and post annealed at higher temperature to improve the crystallinity of the as-synthesized phosphor.

2.2 Instrumentation

Synchrotron angle dispersive X-ray diffraction (Source: BL-12, Indus-2 at RRCAT Indore, India) was recorded to check the crystallinity and the average crystallite size of the samples. Micro-structural characterizations for surface morphology and particle size measurements were carried out using a scanning electron microscope (SEM: QUANTA 200) and Transmission electron microscopy (TEM, TECNAI-20G^2, 200 kV). UC emission was recorded by using a monochoromator (iHR320, Horiba Jobin Yvon) equipped with photomultiplier tube, model no.: 1424M detector. The 976 nm radiation from a diode laser (continuous mode, 2W, power tunable) was used to excite the samples. Photoluminescence excitation (PLE), emission (PL) and lifetime measurements were performed using a Fluorolog-3 spectrofluorometer (Model: FL3-11, Horiba Jobin Yvon). The 266 nm excitation wavelength of a Nd:YAG laser, and CCD (charged coupled device) detector (Ocean Optics, QE 65000) was used for QC measurement.

3. Result and Discussion

3.1 Structural characterization

Initially, the phosphor sample was examined through XRD for structure and particle size. The XRD pattern of the phosphor shows the presence of crystalline cubic phase (JCPDS No.: 25-

1200) of Y_2O_3, which further do not show any change with a variation in Yb^{3+} concentration even up to 15 mol%, see Fig. 1. The material crystallises into cubic phase (a=b=c= 10.60 Å) with *Ia3 (206)* space group. This confirms for an effective doping of Ho^{3+} and Yb^{3+} ions on Y^{3+} cite. The average crystallite size calculated through Debye Scherer formula was found to be more than 100 nm, i.e. phosphor particles evolve in sub-micron size. For the crystallite size calculation, three most intense XRD peaks were selected. The FWHM (full width at half maximum) of these peaks were taken by their Lorentzian peak fitting. The particle size obtained through all the three peaks has been averaged finally. The similar observation is also marked in TEM image (inset to Fig. 1(b)) and particle size lies above 100 nm. Particles are agglomerated in nature and shows nearly spherical morphology, as is visible in SEM image in Fig. 1(b).

3.2 Effect of Li^+ ion on upconversion luminescence

The phosphor sample when irradiated with 976 nm laser gives an intense green emission. The spectrum consists of several peaks with their maximum peaking at 536 nm, 549 nm, 668 nm, and 755 nm, corresponding to $^5F_4 \rightarrow {}^5I_8$, $^5S_2 \rightarrow {}^5I_8$, $^5F_5 \rightarrow {}^5I_8$, and $^5S_2 \rightarrow {}^5I_7$ transitions of the Ho^{3+} ion, respectively, shown in Fig. 2(a).[27,28] The most intense peak is observed in green region at 549 nm. The UC spectrum is further recorded with a variation in Yb^{3+} concentration. Initially, the UC emission intensity is enhanced and attains the maximum intensity for 5 mol% Yb^{3+} concentration, beyond which, the UC emission diminishes considerably. Herein, Yb^{3+} ions acts as the sensitizer for the UC emission of Ho^{3+} ion, as Yb^{3+} is well known for its strong absorption in NIR region. Thus, the incident laser photons are mostly absorbed by Yb^{3+} ion (Ho^{3+} also absorbs 980 nm radiation, called ground state absorption process) and it is promoted to its excited state. The energy from the excited state is later on transferred to the Ho^{3+} ions effectively. Ho^{3+} ions further absorb 980 nm radiation in excited state and are promoted to still high lying excited states (excited state absorption process). Thus increasing

the Yb^{3+} concentration improves the UC emission, but after a certain concentration (5 mol%) quenching effect is observed due to well know energy migration between similar ions.[15] UC mechanism has been verified using well known laser input power dependence process, shown in Fig. 2(b). Slope values for different transitions confirm the involvement of two photon process for red and green transitions. The complete mechanism of the UC emission is shown in the partial energy scheme in Fig. 4. Remarkably, the emission intensity at high input laser powers shows saturation like behaviour. This happens as the increasing pump power does not increase the UC emission with the same rate.[3,29]

Further, an effect of Li^+ ion on the UC emission has been probed. On doping the Li^+ ion in $Y_{1.94}Ho_{0.01}Yb_{0.05}O_3$ phosphor the UC emission intensity increases for a certain concentration and then a decrease in intensity is observed. The best intensity is attained for 5 mol% concentration of Li^+ ion; see Fig. 2(c). In our earlier work on yttrium oxide host, we have already explored various reasons behind the enhancement of UC emission in the presence of Li^+ ion, by using extensive structural characterizationssuch as Fourier transform infrared analysis, and X-ray diffraction (XRD) followed by Le-Bail refinement of the XRD data.[30] These characterizations reveal that the co-doping of Li^+ ion decreases unit cell parameter of Y_2O_3 cubic lattice, increases the particle size, and removes the quenching centers (like OH, NOx , etc.). So, it is concluded that, for Y_2O_3 matrix, Li^+ ion co-doping causes a change in crystal parameter and particle size, but, there is no any change in phase. In addition to this, a review article by our group also summarizes the main facts behind this increase and decrease in emission intensity (both for UC and PL) in several hosts including yttrium oxide too.[25] Li^+ ion is known to have a smaller ionic radius and so when it is incorporated in any matrix, e.g. Y_2O_3, it can either substitute the cation of the matrix or can occupy interstitial sites of the matrix. The probability of occupancy at a particular cite typically depends on the concentration of doped Li^+ ion. At a significantly high concentration

of Li^+ ion, occupancy in the interstitial sites becomes more probable which distorts the matrix, significantly. In few host, changes even in phase and crystal structure are also marked. These all together plays an important role behind the enhancement in the emission to certain concentration, and quenching in emission thereafter. The mechanism of UC emission remains the same. The power dependence plots for different transitions are shown in Fig. 2(d), which shows that two photon processes is responsible for the green and red UC process in Li^+ co-doped samples also. Thus, Li^+ ion co-doping (5 mol%) significantly enhances the UC emission.

3.3 Effect of Li^+ ion on photoluminescence and quantum cutting emission

Photoluminescence excitation (PLE) spectra (monitored for λ_{ems}=549 nm) of the Ho^{3+}, Yb^{3+} co-doped Y_2O_3 phosphor is shown in Fig. 3(a). Y_2O_3 is well known to have its host absorption band in 200-300 nm regime, so excitation spectra have been recorded in the region 300-500 nm only. A large number of sharp peaks, characteristic of Ho^{3+} ion, are obtained. Two peaks originating at 362 nm and 449 nm are the most intense one. All these sharp peaks are due to Ho^{3+} ions. A variation in the intensity of excitation peaks is noted with a varying concentration of Yb^{3+} in the sample. As the concentration of Yb^{3+} increases the intensity of the excitation peaks decreases. The emission spectra of the samples with λ_{exc}= 362 nm and 449 nm are shown in Fig. 3(b) and Fig. 3(c), respectively. Likewise the UC spectrum, PL spectrum also consists of several lines peaking at 536 nm, 549 nm, 656 nm, and 756 nm, corresponding to $^5F_4 \rightarrow {}^5I_8$, $^5S_2 \rightarrow {}^5I_8$, $^5F_5 \rightarrow {}^5I_8$, and $^5S_2 \rightarrow {}^5I_7$ transitions of the Ho^{3+} ion, respectively. The most intense peak is observed in green region at 549 nm. Emission spectra also follow a similar trend to that of excitation spectra with a variation in the concentration of Yb^{3+} ions, i.e. emission also decreases with increasing concentration of Yb^{3+}.

Since, Yb^{3+} is known to have only one excited state ($^2F_{5/2}$) at around 10,000 cm^{-1}, so, in principle there is no direct role of Yb^{3+} under UV excitations (362 nm and 449 nm). It is

expected that this decrease in emission intensity, with an increase in Yb^{3+} concentration, could be due to an energy transfer from Ho^{3+} ions to Yb^{3+} ion. Now few possible ways could be discussed. The first one is the possibility of back energy transfer process. The two levels of Ho^{3+} namely $^5I_5$ (at around 11,200 cm^{-1}) and $^5I_6$ (at around 8,600 cm^{-1}) are lying nearby to the $^2F_{5/2}$ (10,000 cm^{-1}) level of Yb^{3+} ion. However, both the levels are located at a difference of 1200 cm^{-1} or even more which needs the involvement of at least 3 phonons (phonon frequency of Y_2O_3 host is ~400 cm^{-1}) for a resonance energy transfer. Therefore, this process seems less probable. The other possibility is near infrared QC emission through Yb^{3+} ion pair. Further, to probe this QC, the emission due to Yb^{3+} ion ($^2F_{5/2}\rightarrow{}^2F_{7/2}$) was monitored by using CCD detector (it was not possible to detect this emission in PL setup as due to the detection limit of PMT beyond 850 nm). So for this, the 266 nm line of Nd:YAG laser was used as excitation source. Fig. 3(d) shows an intense emission peak in the 950-1050 nm region, which shows an increase in intensity as the concentration of Yb^{3+} increases. The best emission intensity is achieved for 5 mol% concentration of Yb^{3+} ion. A decrease in intensity at 10 mol% Yb^{3+} concentrations may be attributed to self-trapping effect as well as excitation energy migration among adjacent Yb^{3+} ions followed by nonradiative trapping by defects at high Yb^{3+} concentration. In Ho^{3+}/Yb^{3+} couple, NIR QC occurs through de-excitation of $^5S_2$ level of Ho^{3+} via cooperative energy transfer (CET) to Yb^{3+} ion pair. The energy of the $^5S_2\rightarrow{}^5I_8$ transition of Ho^{3+} is nearly double to that of the $^2F_{5/2}\rightarrow{}^2F_{7/2}$ transition of Yb^{3+}, so the excited Ho^{3+} ions can transfer the energy from $^5S_2$ level to the two Yb^{3+} ions. Thus, the QC process in the Ho^{3+}/Yb^{3+} doped phosphor sample could be expressed as $^5S_2\rightarrow{}^2F_{5/2}+{}^2F_{5/2}$. Schematic energy level scheme (partial) shown in Fig. 4 clearly shows different possible ways of transitions, under different excitations i.e. 266 nm, 362 nm and 449 nm, including ET and QC processes. It is obvious from the scheme that, when Ho^{3+} ion is excited by UV light source, ions are excited to higher lying level/host absorption band and further goes through

different radiative and nonradiative relaxations and finally reaches to $^5S_2$ level, from where QC emission is observed as discussed earlier. Similar observation has been reported in other works also; summarized in a review by Liu et al. and references there in.[31]

To realize the effect of energy transfer and also to calculate the energy transfer efficiency/efficiency of QC, decay time analysis has been carried out in detail. Fig. 5(a, b) shows the decay curves of $^5S_2 \rightarrow {}^5I_8$ transition of Ho^{3+} under λ_{exc} = 362 nm and 449 nm, respectively, both with a variation in the concentration of Yb^{3+} ion. The decay curves were fitted well with single exponential following the relation-

$$I = I_0 \exp\left(-\frac{t}{\tau}\right)$$

where, I and I_0 are the intensity at time t and at 0 s, respectively, and τ is the lifetime. The obtained values of lifetime are given in Table I. Further, energy transfer efficiency (η_{ETE}) and the quantum cutting efficiency (QE, η_{QE}) has been calculated. The η_{ETE} is defined as the ratio of Ho^{3+} ions that is depopulate by ET to Yb^{3+} ions over the total number of the Ho^{3+} ions excited. It is estimated by dividing the integrated intensity of the decay curves of Ho^{3+}/Yb^{3+} co-doped samples to that of Ho^{3+} singly doped sample. On assuming that all excited Yb^{3+} decay radiatively, η_{ETE} can be calculated from relation-

$$\eta_{ETE} = 1 - \frac{\tau_x}{\tau_0}$$

Where, τ_x and τ_0 denotes the fluorescence lifetime of Ho^{3+}/Yb^{3+} co-doped and Ho^{3+} singly doped phosphors, respectively, and x stands for the Yb^{3+} concentration. In addition to this, the relation between η_{ETE} and η_{QE} can be taken as below-

$$\eta_{QE} = \eta_{Ho}(1 - \eta_{ETE}) + 2\eta_{ETE}$$

Where, the η_{QE} stands for the quantum cutting efficiency, η_{H0} is the quantum yield of Ho^{3+} transition. Ignoring the nonradiative energy loss by defects and impurities, η_{Ho} is set to 1. The values obtained using these equations are also listed in Table I. Data in Table I are illustrated

through graphs in Fig. 5(c, d) which clearly shows that, the decay time decreases while QC efficiency significantly increases with increasing concentration of Yb^{3+} ion in the sample. The maximum ET and thus QC efficiency is attained for 15 mol% concentration of Yb^{3+} which is about 182 % (λ_{exc}=362 nm). This means that, the absorption of 100 photons (of 266 nm radiation) produces a total of 182 photons (NIR and visible both), out of which 164 photons are emitted in 900-1050 nm (NIR) while the rest of the 18 photons are still emitted in visible region.

As we noted in UC that, incorporation of Li^+ ion significantly changes/enhances the emission intensity, we explored further the effect of Li^+ ion on the PL and QC emission also. For this purpose, 5 mol% Yb^{3+} doped sample ($Y_{1.94}Ho_{0.01}Yb_{0.05}O_3$) was used, as the best UC emission is obtained for this sample. Effect of Li^+ ion on the PL excitation and emission intensity is shown in Fig. 6(a, b). Just like the UC, PL excitation and emission is also enhanced initially (up to 5 mol% Li^+ ion co-doping) and then decreases. This is usual and is well established also. Now, if we look at the QC based emission, interestingly it also enhances the QC based NIR emission and best intensity is observed for 5 mol% concentration of Li^+ ion, see Fig. 6(c). The decay curves of $^5S_2 \rightarrow {}^5I_8$ transition of Ho^{3+} under λexc = 362 nm is shown in Fig. 6(d). The calculated values of decay time, energy transfer efficiency and QC efficiency of Li^+ co-doped samples are given in Table-II. The data concludes that, Li^+ ion co-doping significantly enhances the QC efficiency and more than 8% enhancement in the QC efficiency is noted in presence of Li^+ ion. This enhancement is expected due to an enhancement in PL; due to which population in $^5S_2$ also increases giving rise to an enhancement in cooperative energy transfer from Ho^{3+} ion to Yb^{3+} ion pair.

This type of VU/visible to NIR QC phosphor could be of great potential for c-Si solar cell application. The c-Si solar cells have a poor efficiency in UV and visible (up to green region) and the best conversion efficiency of c-Si solar cell lies in 900-1000 nm region.[31-33]

The simple energy band structure to achieve NIR QC in synthesized phosphor, and utilization of these NIR photons for e-h pair generation in silicon to increase the current, etc are presented in Fig. 7. If an electron is excited from valence band to conduction band by a green photon (λ = 549 nm, hν = 2.26 eV), half of the excited energy will be lost by thermal vibration/relaxation. If the energy of incidence particle is just above the band gap of Si, the energy loss by thermal vibration will be minimized. Thus, in spite of a UV/green photon, two NIR photons (λ = 976 nm, hν = 1.27 eV) emitted through the QC process can just make two electrons exceed the band gap (Eg=1.12 eV) in single-crystalline Si, and the electric current thus doubles theoretically. Accordingly, a high efficiency silicon-based solar cell could be realized through the NIR QC process.

4. Conclusion

Ho^{3+}/Yb^{3+} co-doped yttrium oxide phosphors have been synthesized and characterized for multimodal luminescence. Further, the impact of Li^{+} ion co-doping on the multi-modal emission has been examined, for the first time. Co-doping of Li^{+} ion has been found capable to enhance the QC emission, similar to that of UC and PL emission, and hence the multimodal emission is enhanced. The energy transfer from Ho^{3+} to Yb^{3+} has been calculated whose efficiency is around 82%, and so, the corresponding QC efficiency is 182%. Further, co-doping of Li^{+} ion enhances the QC efficiency for about 8%. This type of NIR QC phosphors has great promises in energy conversion for c-Si solar cell applications.

Acknowledgements

S. K. Singh thankfully acknowledges the financial support by Department of Science and Technology, New Delhi, India in the form of INSPIRE Faculty Award [IFA12-PH-21]. R V Yadav is thankful to DST for JRF. Dr. Thanks are also due to Dr. A. K. Sinha, RRCAT Indore, India, for providing synchrotron angle dispersive X-ray diffraction (Source: BL-12, Indus-2) facility.

References

1 H. Xu, R. Chen, Q. Sun, W. Lai, Q. Su, W. Huang and X. Liu, Chem. Soc. Rev., 2014, 43, 3259-3302.

2 C. Bouzigues, T. Gacoin, and A. Alexandrou, ACS Nano, 2011, 5, 8488-8505.

3 S. K. Singh, A. K. Singh and S. B. Rai, Nanotech., 2011, 22, 275703-275712.

4 T. Kim, N. Lee, Y. Park, J. Kim, J. Kim, E. Y. Lee, M. Yi, B. G. Kim, T. Hyeon, T. Yu and H. B. Na, RSC Adv., 2014, 4, 45687-45695.

5 K. Yan, P. Li, H. Zhu, Y. Zhou, J. Ding, J. Shen, Z. Li, Z. Xu and P. K. Chu, RSC Adv., 2013, 3, 10598-10618.

6 M. West, A. T. Ellis, P. J. Potts, C. Streli, C. Vanhoof, D. Wegrzynekf and P. Wobrauschek, J. Anal. At. Spectrom., 2012, 27, 1603-1644.

7 H. Guo and S. Sun, Nanoscale, 2012, 4, 6692-6706.

8 X. Li, R. Wang, F. Zhang, L. Zhou, D. Shen, C. Yao and D. Zhao, Sci. Rep., DOI: 10.1038/srep03536.

9 Y. Sun, J. Peng, W. Feng and F. Li, Theranostics, 2013, 3, 346-353.

10 S. K. Singh, RSC Adv., 2014, 4, 58674- 58698.

11 X. Yu, W. Bian, T. Wang, D. Zhou, J. Qiu and X. Xu, Cryst. Eng. Comm., DOI: 10.1039/c4ce02521k.

12 H. N. Luitel, R. Chand, T. Torikai, M. Yada and T. Watari, RSC Adv., 2015, 5, 17034-17040.

13 B. Liu, C. Li, P. Ma, Y. Chen, Y. Zhang, Z. Hou, S. Huang and J. Lin, Nanoscale, 2015, 7, 1839-1848.

14 W. He, T. S. Atabaev, H. K. Kim and Y. H. Hwang, J. Phys. Chem. C, 2013, 117, 17894-17900.

15 G. Conibeer, Mater. Today, 2007, 10, 42-50.

16 W. B. Dai, Y. F. Lei, P. Lic and L. F. Xud, J. Mater. Chem. A, 2015, 3, 4875–4883.

17 Z. Hosseini, W. K. Huang, C. M. Tsai, T. M. Chen, N. Taghavinia and E. W. G. Diau, ACS Appl. Mater. Interfaces, 2013, 5, 5397−5402.

18 J. C. G. Bunzli and A. S. Chauvin, Handbook on the Physics and Chemistry of Rare Earths, 2014, 44, 169-281.

19 Y. Z. Wang, D. C. Yu, H. H. Lin, S. Ye, M. Y. Peng, and Q. Y. Zhang, J. Appl. Phys., 2013, 114, 203510-203514.

20 S. Lian, C. Rong, D. Yin and S. Liu, J. Phys. Chem. C, 2009, 113, 6298–6302.

21 J. Ueda and S. Tanabe, J. Appl. Phys., 2009, 106, 043101-043105.

22 J. Zhou, Y. Teng, X. Liu, S. Ye, Z. Maa and J. Qiu, Phys. Chem. Chem. Phys., 2010, 12, 13759- 13762.

23 K. Mishra, S. K. Singh, A. K. Singh, M. Rai, B. K. Gupta and S. B. Rai, Inorg. Chem., 2014, 53, 9561- 9569.

24 F. Auzel, Chem. Rev., 2004, 104, 139-173.

25 A. K. Singh, S. K. Singh and S. B. Rai, RSC Adv., 2014, 4, 27039-27061.

26 S. K. Singh, K. Kumar and S. B. Rai, Appl. Phys. B, 2009, 94, 165-173.

27 A. Pandey and V. K. Rai, Dalton Trans., 2013, 42, 11005–11011.

28 G. H. Dieke, Spectra and Energy Levels of Rare Earth Ions in Crystals, Interscience Publishers, USA, 1968, pp. 253–261 [SBN 470 21390 6].

29 M. Pollnau, D. R. Gamelin, S. R. Luthi, H. U. Gudel and M. P. Hehlen, Phys. Rev. B, 2000, 61, 3337-3346.

30 K. Mishra, S. K. Singh, A. K. Singh and S. B. Rai, Mat. Res. Bull., 2013, 48, 4307-4313.

31 X. Huang, S. Han, W. Huang and X. Liu, Chem. Soc. Rev., 2013, 42, 173-201.

32 T. Trupke, M. A. Green and P. Wurfel, J. Appl. Phys., 2002 92, 1668-1674.

33 G. F. Brown and J. Q. Wu, Laser Photonics Rev., 2009, 3, 394-405.

Table I Variation of lifetime (for $^5S_2 \rightarrow {}^5I_8$ transition of Ho^{3+}), energy transfer efficiency (η_{ET}) and quantum cutting efficiency (η_{QE}) of Ho^{3+} (1 mol%), Yb^{3+} co-doped Y_2O_3 phosphor, with a variation of Yb^{3+} concentration for λ_{exc} = 362 nm and 449 nm.

Yb^{3+} concentration (mol %)	**Life Time** (μs)	**η_{ET}** (in %)	**η_{QE}** (in %)	**Life Time** (μs)	**η_{ET}** (in %)	**η_{QE}** (in %)
	(λ_{exc} = 362 nm)			**(λ_{exc} = 449 nm)**		
0	98. 19	0	100	110.85	0	100
5	55.54	43	143	56.59	49	149
10	37.89	61	161	39.61	64	164
15	17.3	82	182	29.72	73	173

Table II Variation of lifetime (for $^5S_2 \rightarrow {}^5I_8$ transition of Ho^{3+}), energy transfer efficiency (η_{ET}) and quantum cutting efficiency (η_{QE}) of Ho^{3+} (1 mol%), Yb^{3+} (5 mol%) co-doped Y_2O_3 phosphor, with a variation of Li^+ concentration for λ_{exc} = 362 nm.

Li^+ concentration (mol %)	**Life Time** (μs)	**η_{ET}** (in %)	**η_{QE}** (in %)
	(λ_{exc} = 362 nm)		
0	55.54	44	144
5	51.19	47	147
10	50.87	52	152
15	52.16	46	146

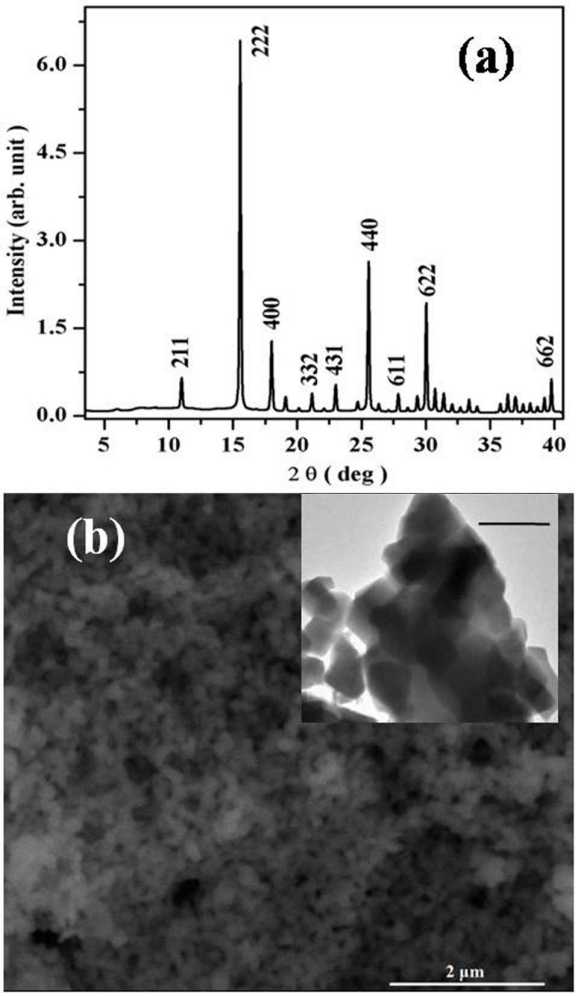

Fig. 1 (a) Synchrotron angle dispersive X-ray diffraction (XRD) pattern of Ho^{3+}/Yb^{3+} co-doped Y_2O_3 phosphor, **(b)** SEM image of the as-synthesized phosphor, and inset shows TEM image of the as-synthesized phosphor (scale bar 200 nm)

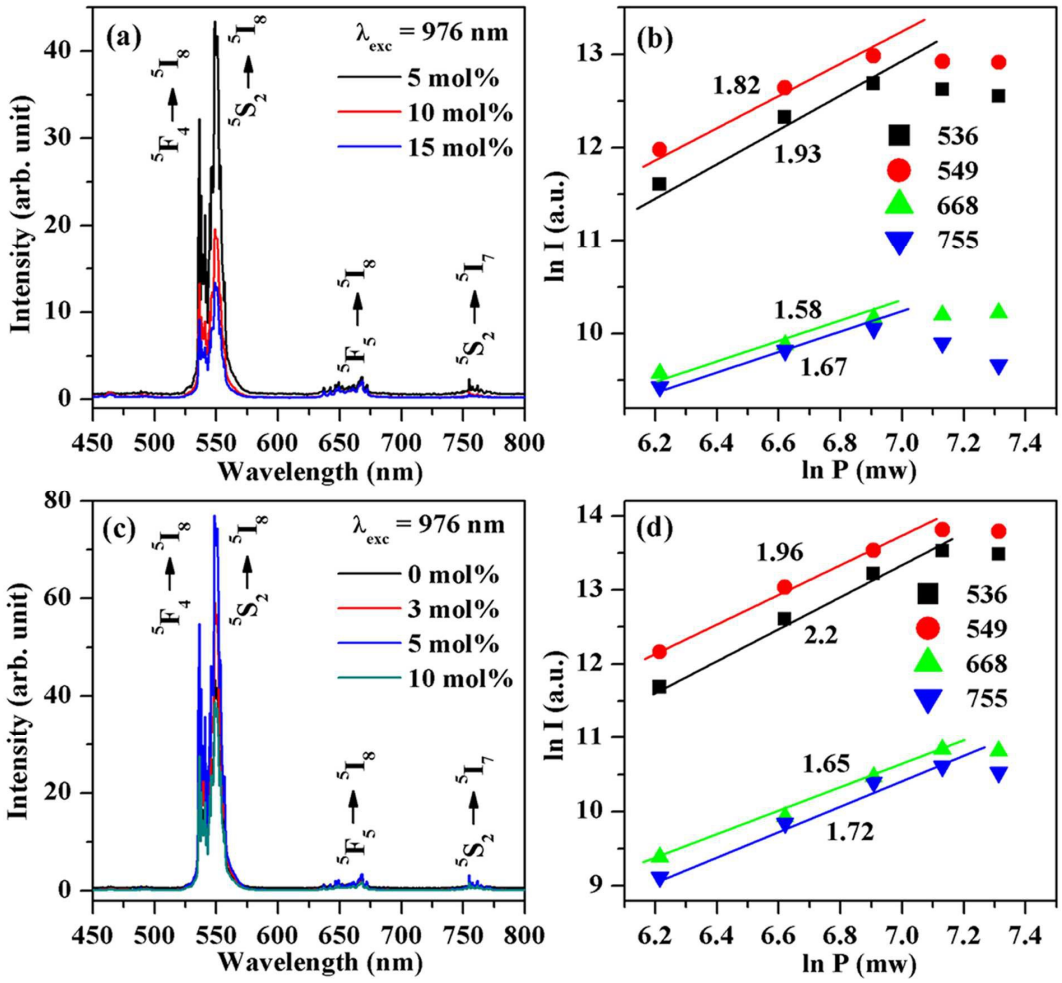

Fig. 2 Upconversion (UC) spectrum (λ_{exc}=976 nm) of **(a)** Ho^{3+} (1 mol%) ion in Y_2O_3 phosphor with varying concentration of Yb^{3+} and **(c)** Ho^{3+} (1 mol%), Yb^{3+} (5 mol%) codoped phosphor with varying concentration of Li^+ ion. **(b, d)** lnI (intensity of UC emission) versus lnP (applied laser input power) plot for UC transitions with Li^+ undoped and Li^+ doped samples, respectively. The slope of these curves (n) gives the number of photons involved in the particular UC transition.

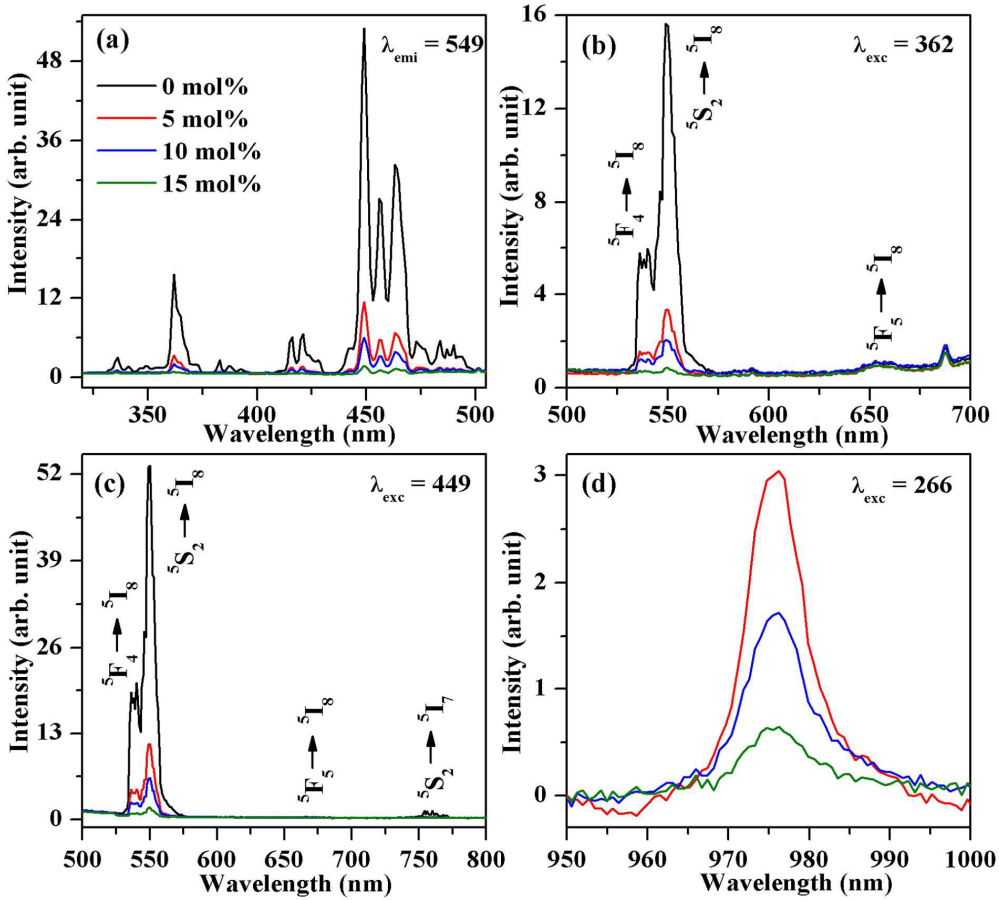

Fig. 3 Photoluminescence excitation and emission spectra Ho^{3+}/Yb^{3+} co-doped Y_2O_3 phosphor with varying concentrations of Yb^{3+} ions. **(a)** Excitation spectra monitored for λ_{ems}=549 nm. Emission spectra for **(b)** λ_{exc}=362 nm, **(c)** λ_{exc}= 449 nm and **(d)** λ_{exc}= 266 nm. Emission spectra with 266 nm show quantum cutting emission.

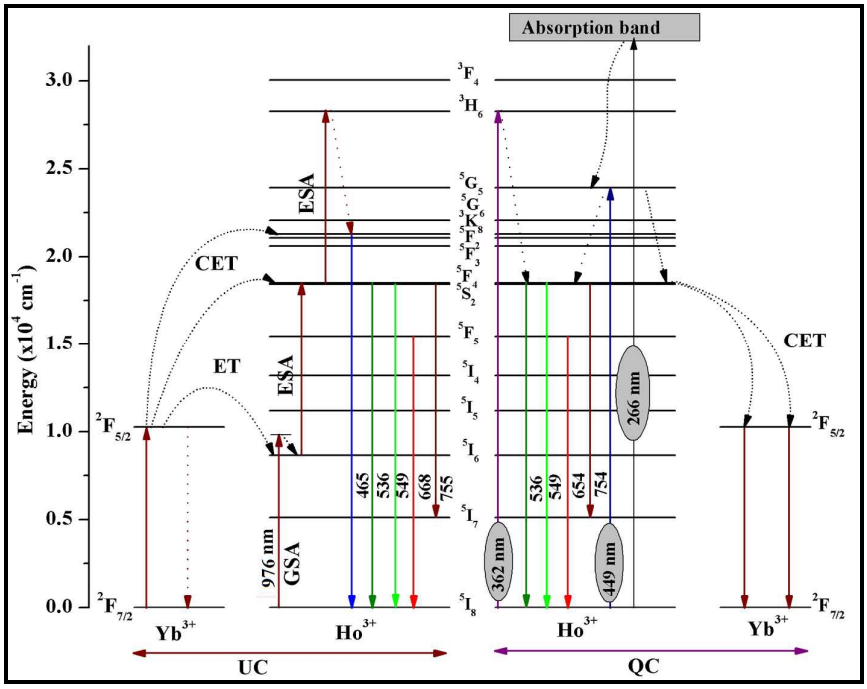

Fig. 4 Partial energy level scheme for Ho^{3+} and Yb^{3+} ions showing different channels involved in multimodal: upconversion, photoluminescence and quantum cutting luminescence

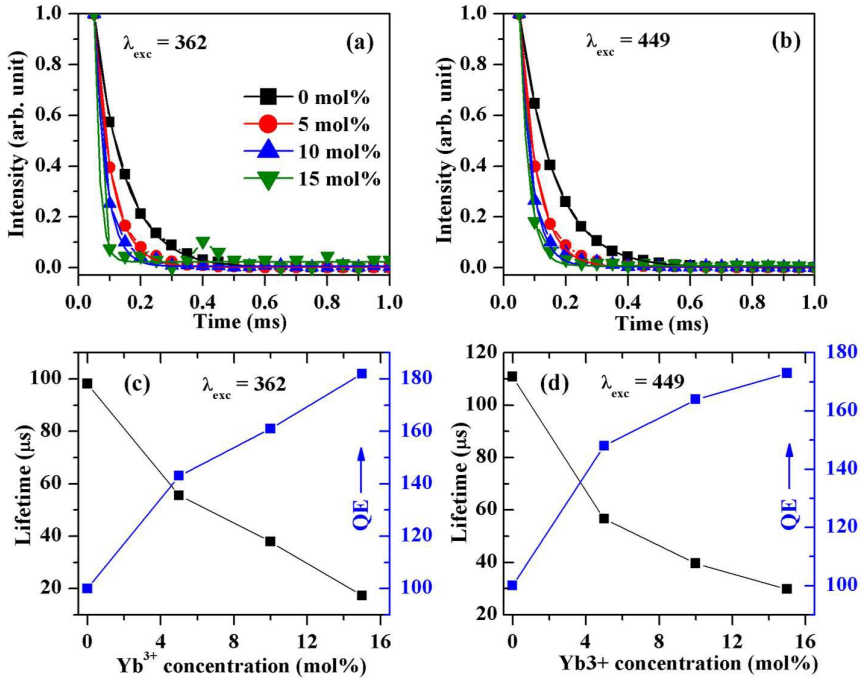

Fig. 5 Decay curves for transition $^5F_4$ /$^5S_2$→$^5I_8$ of Ho^{3+} with varying concentration of Yb^{3+} under- **(a)** 362 nm excitation and **(b)** 449 nm excitation. **(c, d)** Decay lifetimes for transition $^5F_4$ /$^5S_2$→$^5I_8$ of Ho^{3+} versus quantum efficiency (η_{QE}) plotted as a function of Yb^{3+} concentration both for 362 nm and 449 nm excitation.

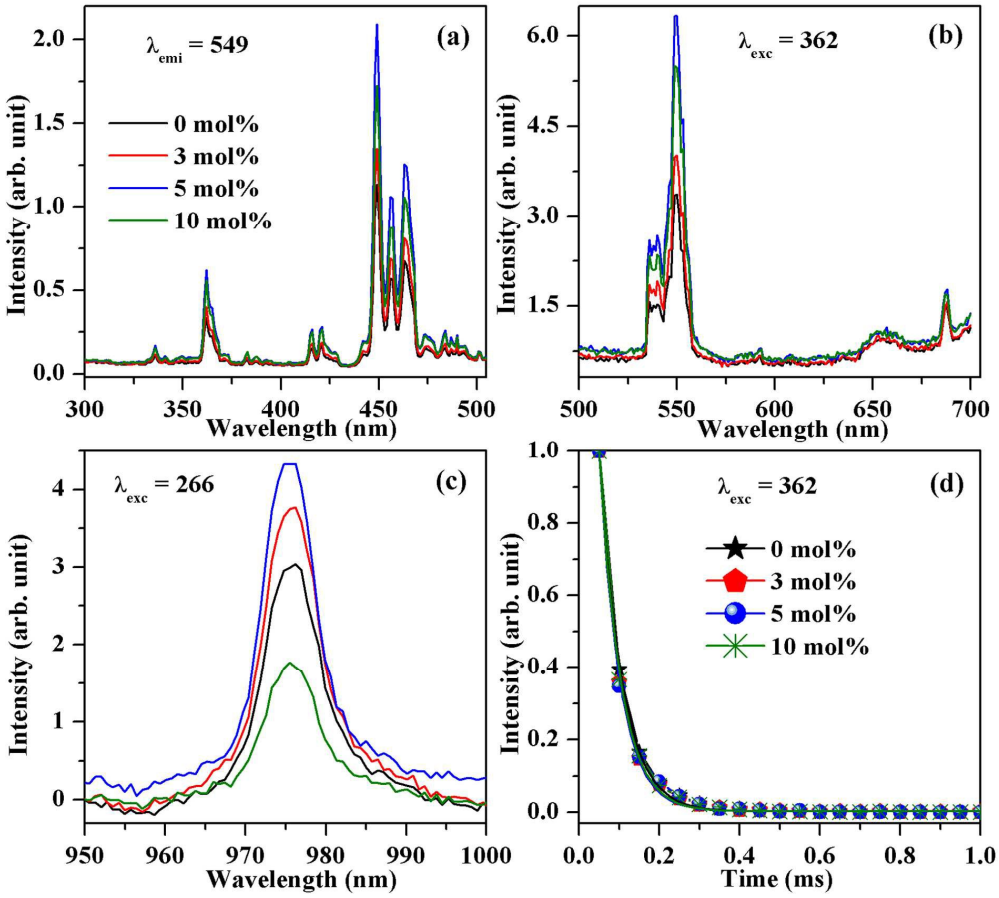

Fig. 6 Photoluminescence excitation, emission, quantum cutting emission and decay curves for Ho^{3+}/Yb^{3+} co-doped Y_2O_3 phosphor with varying concentrations of Li^+ ions. **(a)** Excitation spectra monitored for λ_{ems}=549 nm. Emission spectra for **(b)** λ_{exc}=362 nm, **(c)** λ_{exc}= 266 nm, emission spectra with 266 nm show quantum cutting emission, and **(d)** Decay curves for the transition $^5F_4/^5S_2 \rightarrow {}^5I_8$ of Ho^{3+} ion.

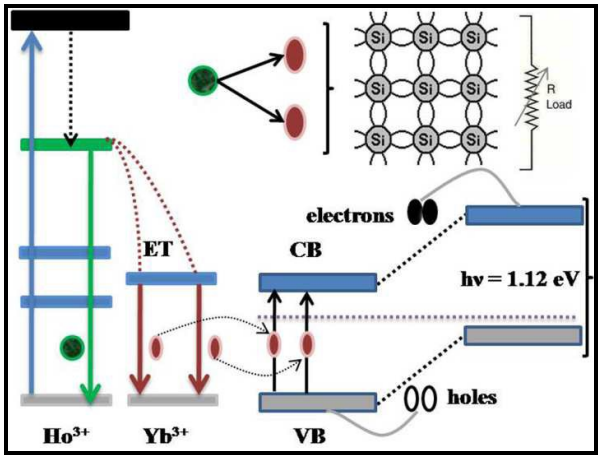

Fig. 7 Application of NIR quantum cutting phosphor in c-Si solar cells. NIR photon emitted through splitting of a green photon (through quantum cutting process) matches well with the band gap energy (1.12 eV) of Si; and so they are absorbed and produce e-h pairs which would contribute well in increasing the solar current.

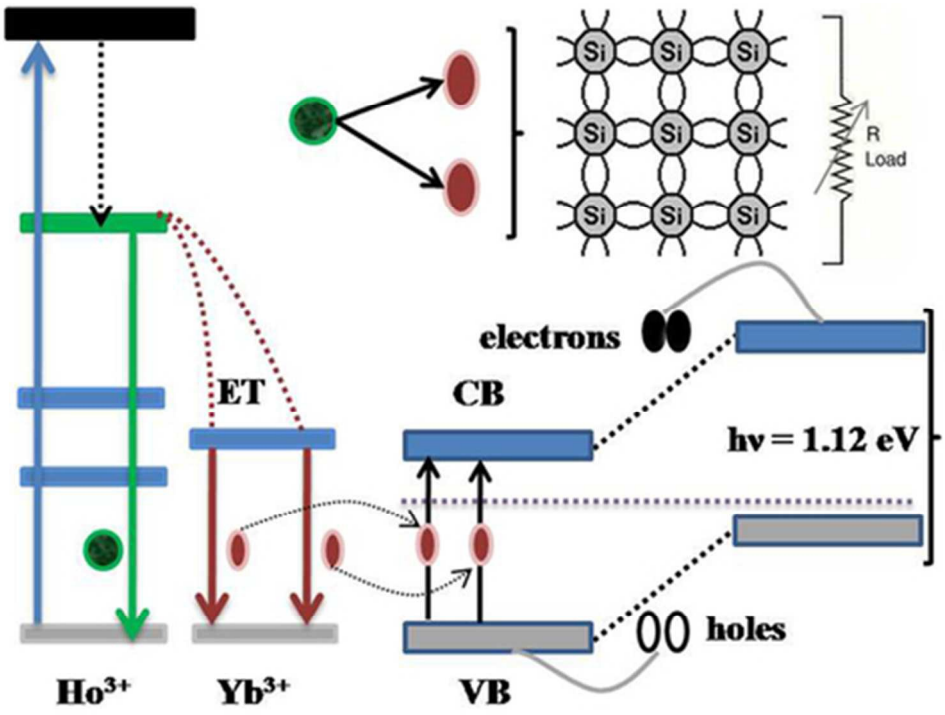

39x30mm (300 x 300 DPI)